Comparison of Modular PEG Incorporation Strategies for Stabilization of Peptide−siRNA Nanocomplexes

Justin H. Lo,[†,‡,#] Ester J. Kwon,[†,#] Angela Q. Zhang,[†,‡] Preeti Singhal,[†] and Sangeeta N. Bhatia*[,†,‡,§,∥,⊥]

[†]Koch Institute for Integrative Cancer Research, MIT, 500 Main Street, Cambridge, Massachusetts 02139, United States
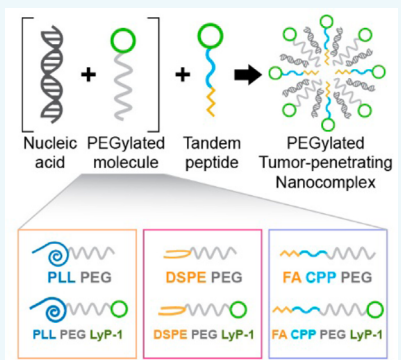
[‡]Harvard−MIT Division of Health Sciences and Technology and [§]Department of Electrical Engineering and Computer Science, MIT, 77 Massachusetts Avenue, Cambridge, Massachusetts 02139, United States

[∥]Department of Medicine, Brigham and Women's Hospital, 75 Francis Street, Boston, Massachusetts 02115, United States

[⊥]Howard Hughes Medical Institute, 4000 Jones Bridge Road, Chevy Chase, Maryland 20815, United States

ⓈSupporting Information

ABSTRACT: Nanoparticulate systems have shown great promise in overcoming the considerable trafficking barriers associated with systemic nucleic acid delivery, which must be addressed to unlock the full potential of technologies such as RNAi and gene editing in vivo. In addition to mediating the cytoplasmic delivery of nucleic cargo and shielding it from nuclease degradation and immunostimulation, nucleic-acid-containing nanomaterials delivered intravenously must also be stable in the bloodstream after administration to avoid toxicity and off-target delivery. To this end, the hydrophilic molecule polyethylene glycol (PEG) has been deployed in many different nanoparticle systems to prevent aggregation and recognition by the reticuloendothelial system. However, the optimal strategy for incorporating PEG into self-assembled nucleic acid delivery systems to obtain nanoparticle stability while retaining important functions such as receptor targeting and cargo activity remains unclear. In this work, we develop substantially improved formulations of tumor-penetrating nanocomplexes (TPNs),

targeted self-assembled nanoparticles formulated with peptide carriers and siRNA that have been shown to mitigate tumor burden in an orthotopic model of ovarian cancer. We specifically sought to tailor TPNs for intravenous delivery by systematically comparing formulations with three different classes of modular PEG incorporation (namely PEG graft polymers, PEG lipids, and PEGylated peptide), each synthesized using straightforward bioconjugation techniques. We found that the addition of PEG lipids or PEGylated peptide carriers led to the formation of small and stable nanoparticles, but only nanoparticles formulated with PEGylated peptide carriers retained substantial activity in a gene silencing assay. In vivo, this formulation significantly decreased accumulation in off-target organs and improved initial availability in circulation compared to results from the original non-PEGylated particles. Thus, from among a set of candidate strategies, we identified TPNs with admixed PEGylated peptide carriers as the optimal formulation for systemic administration of siRNA on the basis of their performance in a battery of physicochemical and biological assays. Moreover, this optimized formulation confers pharmacologic advantages that may enable further translational development of tumor-penetrating nanocomplexes, highlighting the preclinical value of comparing formulation strategies and the relevance of this systematic approach for the development of other self-assembled nanomaterials.

■ INTRODUCTION

Nucleic acid therapies hold great promise for modulating or correcting genetically driven disease processes through modalities such as RNA interference (RNAi),[1] gene delivery,[2] and gene editing through RNA-guided endonucleases.[3] However, nucleic acids are natively incapable of crossing cell and endosomal membranes due to their large size and dense negative charges. Furthermore, nucleic acids are susceptible to enzymatic degradation and can be immunostimulatory when unshielded.[1] Consequently, transportation of nucleic acids to the cell type of interest and subsequently to the correct intracellular compartment requires a delivery vehicle or direct chemical modification. To effectively deliver nucleic acids as cancer therapeutics, our group has designed self-assembled peptide-based nanoparticles, termed "tumor-penetrating nanocomplexes" (TPNs), which

actively target and penetrate into solid tumors in addition to protecting and transporting the nucleic acid cargo.[4] In the TPN system, the nucleic acid-carrying component is a cationic two-domain peptide composed of a C-terminal targeting and penetrating "CendR" peptide, LyP-1,[5] fused to an amphipathic cell-penetrating peptide (transportan)[6] modified by an N-terminal saturated fatty acid tail. We refer to this carrier as a "tandem peptide" due to its structure. The multifunctional targeting moiety, LyP-1, has been used to modify a variety of nanoparticle systems to increase tissue accumulation.[7−10] TPNs are formulated similarly to self-assembling cationic polymer

nanoparticles made from materials such as polyethylenimine and poly-L-lysine, and as such, they share advantages including a large mass percentage of cargo versus carrier, facile formation, and flexibility in the types of nucleic acid cargoes.[11,12] In prior studies, TPNs have mediated robust knockdown in vitro[13] and decreased tumor burden after local, intraperitoneal delivery of siRNA in a mouse model of advanced, disseminated ovarian cancer.[4]

As with many nanoparticle systems, self-assembled particles such as TPNs can be susceptible to aggregation in biological fluids, which leads to mass accumulation in off-target organs with narrow capillary beds or active reticuloendothelial systems, such as the lungs, liver, and spleen. Self-assembled systems that involve electrostatic complexation of highly anionic nucleic acid cargoes also have an added inherent instability relative to other nanoparticle systems, manifesting as decomplexation in the presence of competing components in blood and tissues.[14] Improving the stability of circulating nanocomplexes is therefore critical for maintaining their integrity and longevity en route to target tissues and ultimately minimizing off-target delivery. Particle stabilization strategies have frequently involved incorporation of hydrophilic molecules, most notably polyethylene glycol (PEG), to reduce particle−particle interactions as well as unwanted immune recognition.[15] Successful examples in the realm of self-assembled siRNA delivery technologies include cyclodextrin-containing polymers (using PEGylated hydrocarbons: adamantane-PEG and targeted adamantane-PEG-transferrin),[16] lipidoids (admixed PEG lipids),[17,18] polyethylenimine (direct PEGylation of the carrier),[19] polymeric micelles (PEG as a component of block or graft polymers),[20] and cell-penetrating peptides (partial PEGylation of the Pep-3 peptide carrier).[21] To date, such strategies for overcoming instability have been largely vehicle-specific and empirically determined. Thus, while it is evident that PEG incorporation helps achieve particle stability, the question of how the various physical and chemical properties of candidate PEG-modification strategies impact biological function and in vivo pharmacology remains nonintuitive and unanswered. To inform the decision-making process for selecting a method of PEG incorporation, there is a need for a systematic comparison of modular, easily synthesized stabilizing components that could be deployed across varying platforms.

In this manuscript, we further develop our "tandem peptide" technology for systemic delivery to extend its use to disease sites that are only accessible via the bloodstream. To achieve this goal, we perform a systematic comparison of modular PEGylated components noncovalently mixed with tandem peptides and siRNA during the complexation process to improve the physical and pharmacokinetic properties of TPNs. Specifically, we profile several chemical approaches to achieve this end and synthesize three classes of PEG-containing components that could self-assemble into our nanoparticle formulation: (1) PEG graft polymers, in which the PEG is pendant from a polymer backbone; (2) PEG lipids; and (3) PEGylated peptide carriers, in which the PEGylated additive is a PEG-modified version of the tandem peptide itself. We compare these materials on the bases of particle formation (siRNA encapsulation and particle size), in vitro performance (cellular uptake of siRNA, cell-compartment distribution, and knockdown), and in vivo profile (blood circulation and organ distribution). In particular, we demonstrate that although the addition of either PEG lipids or PEGylated peptide carrier leads to stable nanoparticle formation and robust uptake, only PEGylated peptide preserves RNAi activity, indicating the need for a multidimensional analysis of stabilization strategies. Furthermore, particles incorporating PEGylated peptide display improved pharmacokinetics with enhanced initial blood circulation and reduced off-target organ accumulation. The capacity to yield nanoparticles with this set of traits is imperative for the success of tumor-penetrating peptides in the setting of systemic administration and applicable to the delivery of siRNA or other nucleic acids to most types of solid tumors. More generally, these successful modular strategies may instruct the stable formulation of other self-assembled nanoparticle systems using simple bioconjugation techniques.

■ RESULTS

Modular PEG Component Candidates. For a framework for comparing modular strategies for nucleic acid nanocomplex stabilization, we designed three approaches with contrasting mechanisms of PEG incorporation: (1) poly-L-lysine−PEG, which incorporates via electrostatic interactions, (2) distearoylphosphatidylethanolamine (DSPE)−PEG, expected to incorporate into the particle via hydrophobic interactions, and (3) palmitoyl-transportan−PEG, expected to incorporate via a combination of hydrophobic and ionic interactions (Figure S1). For each of the three PEGylated compounds, we used a 5 kDa PEG chain, a length widely used in the literature[22] and successfully applied to several nanoparticle systems in our group.[23,24] We were also interested in determining whether it is beneficial to display the targeting moiety on the distal end of the PEG chain, as such a modification could potentially improve cell-targeting functionality. For this purpose, we generated both untargeted and targeted (containing covalently linked LyP-1, the same C-terminal "CendR" peptide on the mTP-LyP-1 tandem peptide) conjugates of each class of PEG. We explored several approaches to forming the PEGylated tumor-penetrating nanocomplexes (TPNs) and found that only one order of operations resulted in stabilized nanoparticles. In this successful protocol that we applied to each of the particle variants, we first mixed one of the six PEG-containing components with the siRNA in water, added an equal volume of the tandem peptide carrier (myr-transportan−LyP-1) in water, and finally diluted the particles in the appropriate buffer or media (Figure 1).

Physical Properties of TPNs Modified with Modular PEG-Containing Components. We first compared the physical properties of PEGylated TPNs to identify the formulation space in which TPNs can maintain nanoparticle stability in ionic solutions (PBS) while still fully encapsulating the siRNA cargo. In these experiments, we maintained a fixed 15:1 ratio of peptide−siRNA (N-to-P ratio of 2.5) and varied the PEGylated component from 0:1 to 15:1 PEG−siRNA to achieve final peptide−PEG−siRNA ratios ranging from 15:0:1 to 15:15:1. All three chemistries, targeted or not, showed complete encapsulation of free siRNA on the basis of electrophoretic mobility shift assays (Figure S2). However, only the DSPE−PEG and pTP−PEG derivatives were able to prevent aggregation of the particles, defined as hydrodynamic diameters exceeding 400 nm after 30 min of incubation. Specifically, DSPE−PEG particles were observed to be stable at PEG content ratios of 15:2.5:1 and greater, and pTP−PEG particles were stable at PEG content ratios of 15:5:1 and greater (Figure 2A−F). We were particularly interested in particles with diameters of ∼100−200 nm or smaller, which fit within the estimated endothelial gap or fenestration sizes present in tumor vasculature[25] and take advantage of the improved effective diffusion coefficients that come with reduced particle diameter.[26] To satisfy this criterion, we determined that the minimum PEG content was 15:2.5:1 for
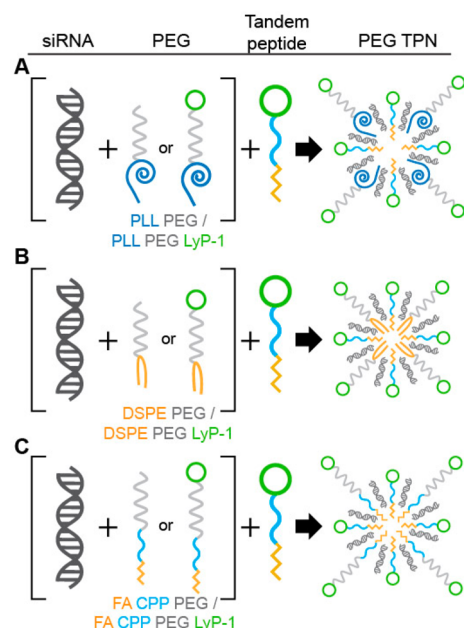
Figure 1. Schematic of approach to formulating PEGylated TPNs. (A−C) Schematic representation of the formation of PEGylated TPNs through incorporation of (A) PEG graft polymers (PLL), (B) PEG lipids (DSPE), and (C) PEGylated peptide carriers (tandem peptide: FA-CPP (pTP)), either untargeted or targeted with the tumor-penetrating peptide LyP-1 (shown in green). In all cases, PEGylated TPNs are synthesized (left to right) by first mixing siRNA cargo with one of the six PEGylated components at specified ratios and then subsequently adding the tandem peptide component to form the final particle. The schematic of the formed particles reflects the contents of the nanocomplex rather than the precise arrangement or shape of the particle.

DSPE−PEG, 15:5:1 for DSPE−PEG−LyP-1, and 15:7.5:1 for both pTP−PEG derivatives. To visualize the resulting particles, we obtained TEM micrographs of representative stabilized 15:15:1 DSPE−PEG and pTP−PEG TPNs, which appeared as globular structures (Figure S3). However, the inherent low contrast of the TPN components and susceptibility to drying artifacts limit quantitative interpretation from this technique. To further investigate the consequences of PEG incorporation on the physical properties of TPNs, we measured the ζ potential of

the six particle types at 15:7.5:1 and 15:15:1 ratios (Figure 2G). The stabilized DSPE−PEG-derivative and pTP−PEG-derivative particles overall had surface potentials closer to neutral (all <10 mV in magnitude) compared to the native non-PEGylated particles, consistent with surface stabilization with neutral PEG. The DSPE−PEG derivatives contributed to a slightly negative surface potential in keeping with the negative charge of the fatty acid. In contrast, pTP−PEG-derivative particles were slightly positive, with pTP−PEG−LyP-1 particles moreso than pTP−PEG particles, which we anticipated on the basis of the display of the cationic LyP-1 peptide at the distal end of the pTP−PEG.

Recognizing that the preceding studies focused on stability of the particles specifically in the face of ionic challenge, we next performed sizing studies in the context of 30% exosome-free fetal bovine serum. Here, we found that representative particles in the stable regime, the 15:15:1 pTP−PEG−LyP-1 TPNs, formed equivalent particles in serum and PBS; additionally, incubation at room temperature or at body temperature resulted in only slight changes in particle diameter (Figure S4). Lastly, we investigated stability of DSPE−PEG and pTP−PEG-formulated nano-complexes against decomplexation by a competing anionic polymer, polyglutamic acid (Figure S5). After formulation, the PEGylated TPNs were incubated with increasing amounts of poly glutamic acid and siRNA release was measured by a gel mobility shift assay. We found that nanocomplexes stabilized by DSPE−PEG released siRNA at lower concentrations of polyglutamic acid compared to results when nanoparticles were stabilized by pTP−PEG. In summary, modification of TPNs with DSPE−PEG and pTP−PEG derivatives resulted in ratio-dependent stabilization of the particles without compromising siRNA encapsulation.

Preservation of Silencing Function in a Subset of PEGylated TPN Formulations. Excess PEG has been shown previously to have the capacity to interfere with delivery or function of siRNA cargo.[27−29] Therefore, we next characterized the functional aspects of PEGylated TPNs in vitro. Because PLL−PEG derivatives were not able to stabilize nanoparticles, we focused on testing the DSPE−PEG and pTP−PEG derivatives, particularly at the 15:15:1 ratios that yielded the smallest particle sizes. The OVCAR-8 ovarian cancer cell line aberrantly expresses p32 on its surface, which acts as the receptor for the LyP-1 targeting peptide, thus making these cells suitable models for testing LyP-1-targeted PEG TPNs.[4] We first assessed
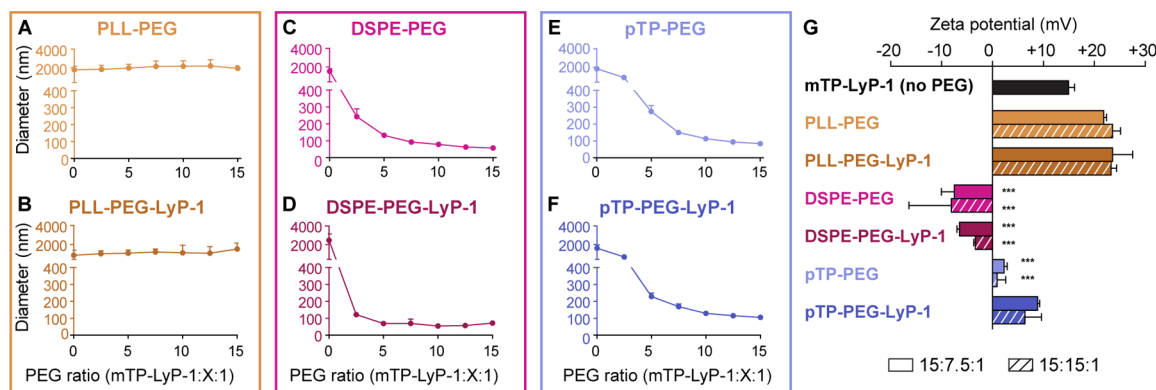

Figure 2. Physical properties of PEGylated TPNs. (A−F) Hydrodynamic diameters of TPNs formed in 1× PBS and formulated with (A) PLL−PEG, (B) PLL−PEG−LyP-1, (C) DSPE−PEG, (D) DSPE−PEG−LyP-1, (E) pTP−PEG, or (F) pTP−PEG−LyP-1. Sizes were determined by dynamic light scattering; particles with diameters of >∼400 nm are unstable. (G) Surface ζ potentials of PEGylated TPNs at 15:7.5:1 and 15:15:1 ratios. Three asterisks indicate $p < 0.005$ for statistical difference compared to the native (non-PEGylated) particles by one-way ANOVA with Tukey post-test.

the association of 15:15:1 PEGylated particles with the cells 24 h after dosing with TPNs, quantifying both near-infrared-labeled siRNA cargo and TAMRA-labeled peptide fluorescence by flow cytometry. This experiment showed that the association of siRNA with cells is increased in the case of TPNs with DSPE– PEG or pTP–PEG derivatives relative to non-PEGylated particles, whereas peptide association is not substantially altered (Figure 3A). To determine the localization of siRNA at the cellular level, we visualized cells using fluorescent microscopy 24 h following TPN dosing. Control non-PEGylated TPNs formed punctate aggregates in cells (Figure 3B, bottom left) as well as extracellular formations observed prior to washing and imaging the cells (not shown). In contrast, all the PEG-containing TPN formulations were notable for the absence of punctate aggregates while still yielding diffuse cytoplasmic siRNA distribution (Figure 3B, center and right panels). Finally, to evaluate the function of this cytoplasmic siRNA, we compared the knock-down efficiency of siRNA targeting a firefly luciferase reporter stably expressed in the OVCAR-8 cells when that siRNA was delivered by particles with various levels of PEG incorporation (Figure 3C). To control for cell number in each well, we normalized luciferase activity relative to the total protein content per well. The knockdown of luciferase activity achieved by DSPE–PEG- and DSPE–PEG–LyP-1-containing TPNs was around 10–20%. In contrast, significantly greater knockdown was observed when either pTP–PEG or pTP–PEG–LyP-1 particles were used as the delivery vector, with >20% knockdown achieved by all pTP–PEG conditions and ∼50–60% knockdown observed across all ratios of pTP–PEG–LyP-1-containing TPNs, the latter being equivalent to the level of knockdown mediated by unmodified TPNs in this reporter system.

Improved Blood Circulation and Organ Biodistribution with PEG-Containing TPNs. On the basis of the favorable physical properties and knockdown capacity of pTP–PEG and pTP–PEG–LyP-1 TPNs, we next sought to establish the in vivo profile of these particles. Although the circulatory half-life of intravenously administered nanocomplexes is typically quite brief and often comparable to that of free siRNA,[30,31] we hypothesized that these PEG modifications would modulate the circulatory kinetics by preventing premature clearance. Indeed, in mice injected with TPNs via tail vein ($n = 5$ per condition) and monitored by serial blood draws over 160 min, both PEG-containing formulations showed increased blood concentrations in the initial phase through ∼20–40 min after injection, relative to unstabilized TPNs (Figure 4A). In later phases (80 min and after), no differences in blood concentration were noted. To investigate the mechanisms underlying these circulatory kinetics, we looked to complement activation on the basis of literature showing complement activation by nanoparticles as a mechanism of clearance from the bloodstream, as well as the potential for PEGylation of particles to modulate complement response.[32–34] We assayed for complement activation associated with TPNs by incubating unstabilized, pTP–PEG, and pTP–PEG–LyP-1 TPNs with human plasma in vitro using the approximate concentration and conditions that would occur in the blood-stream, followed by measurement of C3a and C5a levels (representative products of complement activation). We found that neither C3a nor C5a were elevated by native TPNs, nor were these levels significantly different with the pTP–PEG and pTP–PEG–LyP-1 particles (Figure S6). We then sought to determine whether the different primary half-life of the PEGylated particles might be linked with differential capture in various organs. To quantify the effect of PEG incorporation on organ accumulation,
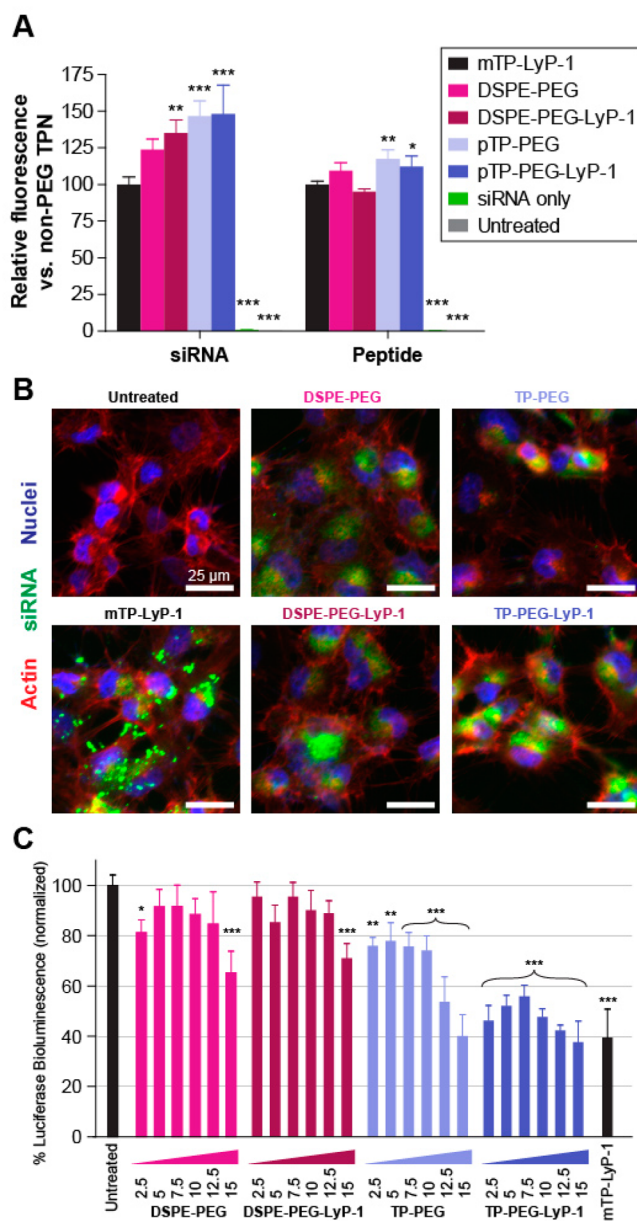

Figure 3. In vitro functionality of PEGylated TPNs. (A) 24 h OVCAR-8 cell uptake of VivoTag750-labeled siRNA and TAMRA-labeled peptide incorporated into PEGylated TPNs, formed at a 15:15:1 peptide–PEG–siRNA molar ratio. Quantified using flow cytometry and normalized to mTP-LyP-1-only particles. Statistical significance by one-way ANOVA vs mTP-LyP-1 particles. A single asterisk indicates $p <$ 0.05; two asterisks indicate $p < 0.01$; three asterisks indicate $p < 0.005$. (B) Representative fluorescent microscopy of OVCAR-8 cells showing localization of DyLight-647-labeled siRNA (green). Actin filaments (red: Alexa Fluor 488-phalloidin) and nuclei (blue: Hoechst) were stained to show cellular compartments. Scale bar: 25 μm. (C) 48 h knockdown of firefly luciferase reporter protein in OVCAR-8 ovarian cancer cells by TPNs with varying ratios of PEG components admixed; measured by bioluminescence. Statistical significance of each condition vs media-only untreated control determined by one-way ANOVA. Single asterisk: $p < 0.05$; two asterisks: $p < 0.01$; three asterisks: $p <$ 0.005.

we performed a biodistribution study in mice bearing subcutaneous flank xenografts of MDA-MB-435 human tumor cells. At 3 h after intravenous administration of the PEGylated TPNs, we measured significant reductions in off-target
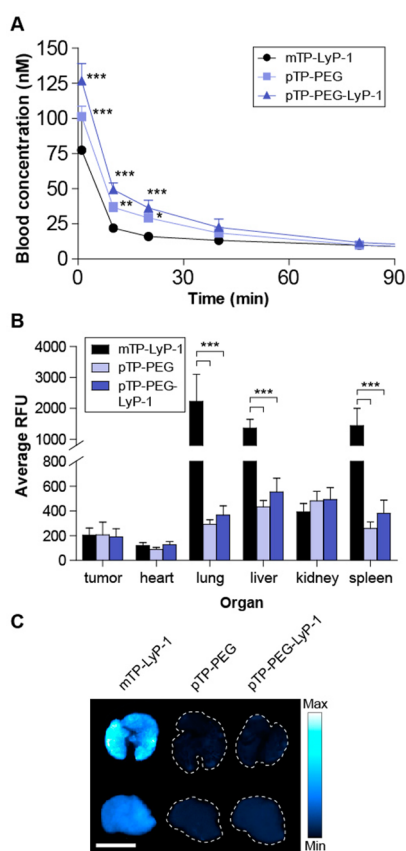
Figure 4. In vivo properties of PEGylated TPNs. (A) Circulation kinetics of unmodified TPNs and PEG TPNs incorporating pTP−PEG or pTP−PEG−LyP-1 at 15:15:1 peptide−PEG−siRNA ratios, read by near-infrared fluorescence of labeled siRNA. Statistical significance determined by two-way ANOVA with Bonferroni post-test. Single asterisk: $p < 0.05$, two asterisks: $p < 0.01$, three asterisks: $p < 0.005$. $n = 5$ per condition. (B) Organ biodistribution of intravenously administered unmodified TPNs vs PEG TPNs with pTP−PEG or pTP−PEG−LyP-1 at 15:15:1 peptide−PEG−siRNA ratios, assessed 3 h after injection. Statistical significance determined by two-way ANOVA with Bonferroni post-test. The three asterisks indicate $p < 0.005$. $n = 7$ per condition. (C) Representative near-infrared scans of lungs (top row) and liver lobes (bottom row) from the organ biodistribution experiment presented in panel (B). Scale bar: 1 cm.

pulmonary (8-fold in pTP−PEG and 6-fold in pTP−PEG−LyP-1), splenic (6-fold and 4-fold, respectively), and hepatic (3-fold and 2-fold) accumulation of siRNA cargo compared to non-PEGylated controls (Figure 4B,C). Meanwhile, siRNA accumulation remained unchanged in the tumors themselves. Therefore,

the relative on-target accumulation was improved with the PEG-containing formulations. Overall, pTP−PEG and pTP−PEG−LyP-1-containing TPNs maintained higher blood concentrations during the first half-hour after administration and, moreover, resulted in greatly decreased distribution into off-target organs.

■ DISCUSSION

The goal of this work was to compare modular PEG incorporation strategies to establish basic principles for electrostatically complexed nanoparticles intended for systemic administration of siRNA cargo. In these studies, we contrasted three different classes of PEG incorporation strategies (PEG graft polymers, PEG lipids, and directly PEGylated peptide carriers) in terms of their ability to form particles with desirable physicochemical properties while retaining silencing activity, as summarized in Table 1. To this end, our experiments found that TPNs formulated with PEG−peptide derivatives exhibited particle stability in physiologically relevant solutions and packaging of siRNA cargo while retaining full knockdown efficiency. These TPN formulations were further examined for stability after intravenous administration in mice and displayed improved circulation and biodistribution profiles.

Comparison among the different PEG-incorporating strategies sheds light on possible principles at play in the formation of self-assembling nucleic acid carriers. In the case of the DSPE−PEG and PEG−peptide derivatives that yielded salt-stable particle formulations, adding increasing molar ratios of PEG reduced particle size without compromising incorporation of the siRNA, although the optimal ratio required for stable particle formation varied on the basis of PEG carrier (Figure 2). As demonstrated by the curves depicting size versus PEG ratio, these modular strategies enable tunability of mean particle size to within a narrow, predictable range while using a fixed set of starting components, eliminating the need for synthesizing separate chemical entities during optimization. Although peptide−PEG and PLL−PEG are both amino-acid-based components with siRNA-binding capacity, only the peptide−PEG derivatives stabilized particles in the range tested. These empiric differences are likely due to the architecture of the two strategies: peptide−PEG was synthesized such that the peptide and PEG portions are oriented linearly, while PLL−PEG was synthesized by grafting PEG onto the side chains of PLL.

Another important dimension of our findings is that the physical properties did not completely correspond with the functional activity of the various formulations of TPNs. Although stable particles can be achieved by a variety of methods, it has been documented that stabilization often comes at the expense of knockdown activity in siRNA carriers.[27−29] Both DSPE−PEG and peptide−PEG incorporation strategies generate stable

Table 1. Summary of Results Comparing Three Modular Strategies for siRNA Nanoparticle Stabilization in Nontargeted (− LyP-1) and Targeted (+ LyP-1) Forms[a]

	PLL−PEG		DSPE−PEG		pTP−PEG	
	− LyP-1	+ LyP-1	− LyP-1	+ LyP-1	− LyP-1	+ LyP-1
encapsulates siRNA cargo	yes	yes	yes	yes	yes	yes
forms <200 nm stable nanoparticles	no	no	15:5:1 and higher	15:2.5:1 and higher	15:7.5:1 and higher	15:7.5:1 and higher
mediates cell association of siRNA			yes	yes	yes	yes
maximum silencing activity in reporter assay			∼25%	∼30%	∼60%	∼60%
improves circulatory profile in systemic administration					yes	yes
reduces off-target organ accumulation					yes	yes

[a]Molar ratios are expressed as peptide carrier−PEG component−siRNA.

particles and exhibit similar levels of cell association, but the activity of peptide−PEG stabilized particles outperformed their DSPE−PEG counterparts at similar ratios (Figure 3C), even after accounting for variables like particle size. In particular, the only formulation that performed on par with unstabilized formulations was the targeted peptide−PEG−LyP-1. In the context of lipid-based carriers such as liposomes, DSPE−PEG is often an indispensable part of the formulation, but within the scope of self-assembled nanocomplexes examined here, we observed considerable decreases in knockdown activity compared to unmodified TPNs. The difference in activity between DSPE−PEG and peptide−PEG nanocomplexes was not due to changes in the total material taken up by cells, as determined by quantification of cellular uptake using flow cytometry (Figure 3A). It is possible that the PEG moiety affected siRNA release during various stages of delivery or the accessibility of siRNA following endosomal escape. Such differences were suggested by the polyanion exchange experiment (Figure S5), in which DSPE−PEG TPNs released siRNA cargo at a lower concentration threshold of competing polyglutamic acid compared to peptide−PEG TPNs. Furthermore, the functional activity of the various formulations depended not only on the type of derivative but also the relative ratio of PEG concentration to carrier peptide concentration. Improvements with additional PEG were seen in several PEG constructions, but we also noted, in line with studies in the literature, that particles formed purely of PEGylated material and siRNA show essentially no function (data not shown).[21,27]

In our animal studies, we observed increased initial circulatory concentrations of siRNA with PEGylated TPNs (Figure 4A), consistent with the concomitant reduction in nonspecific organ accumulation (Figure 4B,C) and with our in vitro demonstration of size stability following serum incubation through at least 1 h (Figure S4). Neither the non-PEGylated nor PEGylated TPNs appeared to trigger complement activation in plasma in vitro (Figure S6). While TPNs, as with most nanoparticles, display repetitive epitopes that can be conducive to complement activation, the minimal empirically observed interaction of the particles with the complement cascade may be related to the zwitterionic and amphipathic character of all TPNs and large size of the non-PEGylated particles; further properties including specific surface chemistry and particle shape may also have a bearing on complement activation.[34,35] We note that our experiments do not rule out more nuanced immunological reactions (for instance, classical pathway activation from antibodies raised after repeated dosing of TPNs or cross-talk between toll-like receptors and complement). Nevertheless, the results from our complement activation study suggest that observed differences in circulation properties are likely due to other ramifications of altering surface charge and particle size on interactions with plasma, cells, and ECM independent of the complement cascade.

We did not observe changes in tumor accumulation based on adding targeting to the PEG component, likely because the core carrier (mTP-LyP-1) was targeted in all formulations. Similar uptake between formulations was also reflected in the cellular association/uptake studies (Figure 3A). Nevertheless, knockdown activity of peptide−PEG−LyP-1 nanoparticles was higher in vitro in comparison to results from peptide−PEG nanoparticles (Figure 3C), suggesting that there is an important role for targeting in the steps beyond organ-level localization. This phenomenon is consistent with findings in a previous report, which described that the addition of transferrin on the surface of nanoparticles did not increase bulk accumulation into transferrin receptor positive tumors but was important for localizing material within the tumor cells.[36] The PEG-targeting strategy represented here can be easily adapted for the introduction of alternative targeting moieties using the bio-orthogonal click chemistry handle, such as folate,[37] transferrin,[16,38] and GalNAc.[39]

Another key aspect of biodistribution studies is the issue of nonspecific accumulation, known in the literature to be a major source of nanoparticle toxicity.[15,22] We were encouraged by the accumulation reductions we observed in lung, liver, and spleen with PEG-containing formulations of TPNs. Entrapment in the lung capillaries, a first-pass effect that is often the consequence of large particle size or exposed cationic charges, was dramatically reduced by addition of either LyP-1 targeted or untargeted peptide−PEG components, achieving up to an 8-fold decrease. This effect was confirmed by imaging, in which mice dosed with unmodified TPNs showed pronounced medium- and small-vessel fluorescence that was absent in the lungs of mice dosed with PEGylated TPNs (Figure 4C). Furthermore, it is likely that the altered surface characteristics following incorporation of hydrophilic PEG molecules, as well as smaller particle size, resulted in reduced recognition by the RES system in the liver and spleen, a well-known mechanism for rapid nanoparticle clearance.[40]

■ CONCLUSIONS

As a whole, our study offers a roadmap for future iterations of peptide-based nucleic acid carriers, even as targeting domains and cargoes are replaced and the applications of the technology are broadened. We have presented bioconjugate strategies that are easily adaptable for any peptide sequence and accessible to nonchemists. To evaluate these strategies, we have also developed a battery of metrics that are generally available to many laboratories to discriminate between formulations designed for eventual systemic delivery. Importantly, the use of a combination of these metrics is key, as we have learned that although strategies for stabilization may yield stable particles as designed, only a subset may maintain functional activity. While many nanoparticle characteristics cannot be predicted from first principles, necessitating empiric testing with a comprehensive battery of tests as we have performed, the synthesis of our data with studies available in the literature suggests that engineering PEG incorporation to preserve the architecture of the nanoparticle system may be a useful starting tactic for improving the stability, activity, and pharmacokinetics of the resulting nanocomplexes. Accordingly, an important factor in the approach to incorporating agents is taking into account the dominant physical interactions that govern particle formation: in the case of this work, harnessing the properties of transportan−siRNA interactions to incorporate PEG into TPNs was most successful, whereas in the case of a lipid−nucleic acid nanoparticle, lipid−PEG conjugates often provide optimal stability. We believe that the principles contributing to TPN stabilization may be extended more broadly to other electrostatically assembled systems, as any nanoparticulate nucleic acid delivery platform designed for clinical applications will likely incorporate PEG or other stabilizing molecules as part of the formulation.

■ EXPERIMENTAL PROCEDURES

siRNA. All siRNAs were synthesized by Thermo Scientific and Dharmacon. A pair of sequences were used for these studies: negative control nontargeting siRNA (siNC, based on a control

sequence published by Qiagen), sense strand 5′-UUCUCC-GAACGUGUCACGUUU-3′; and firefly luciferase siRNA (siLuc), sense strand 5′-CUUACGCUGAGUACUUCGA-3′. All siRNAs were synthesized with dTdT overhangs. For the gel mobility shift assay and microscopy imaging, siLuc was synthesized with a 5′ DyLight 677 fluorophore or 5′ DyLight 647 fluorophore, respectively.

Near-Infrared siRNA Labeling. For biodistribution studies, siNC with 5′ and 3′ amine termini was labeled with VivoTag-S750 amine-reactive dye (PerkinElmer) by reacting the siRNA with a 10:1 molar ratio of dye to siRNA for 1 h shaking at room temperature. siRNA was purified twice by precipitation. siRNA yield and labeling efficiency were quantified on a NanoDrop spectrophotometer (Thermo Scientific). Final labeling was ∼2.4 dyes per siRNA duplex.

Peptides. Myristoyl-transportan–LyP-1 tandem peptide was synthesized by CPC Scientific (sequence: myr-GGWTLNSA-GYLLGKINLKALAALAKKIL-GGGG-CGNKRTRGC, Cys–Cys bridge). Fluorescently labeled peptide was synthesized by Selleckchem, with a tetramethylrhodamine (TAMRA)-tagged lysine inserted into the glycine spacer. FAM-labeled LyP-1 bearing an azide (azidoacetyl-GGG-cyclo-(EGNKRTRGK)), FAM-labeled LyP-1 bearing a cysteine (C-K(5FAM)-C6-cyclo-(CGNKRTRGC)) and transportan bearing a C-terminal cysteine (myristic acid-GGWTLNSAGYLLGKINLKALAA-LAKKILC) were synthesized by CPC Scientific, Inc.

DSPE–PEG and DSPE–PEG–LyP-1 Synthesis. DSPE–PEG–MAL 5K (Nanocs) was reacted with 1.1 equiv of cysteine-bearing LyP-1 in 50 mM triethylamine, N,N-dimethylformamide and stirred overnight. The final conjugate was purified into water using a PD-10 desalting column (GE Healthcare Life Sciences). DSPE–PEG 5K was purchased from Avanti Polar Lipids.

pTP–PEG and pTP–PEG–LyP-1 Synthesis. OPSS–PEG–SVA 5K (Laysan Bio) was reacted with 5 equiv of N-[(1R,8S,9s)-bicyclo[6.1.0]non-4-yn-9-ylmethyloxycarbonyl]-1,8-diamino-3,6-dioxaoctane (Sigma) for 3 h at room temperature. The resulting conjugate was dialyzed using a 3500 MWCO membrane and lyophilized. This product was dissolved in DMF and reacted with 1.2 equiv of transportan bearing a C-terminal cysteine for 3 h at room temperature. A total of 1.2 equiv of LyP-1-azide was added and reacted further overnight. The final product was dialyzed using a 3500 MWCO membrane into water. pTP–PEG was synthesized by omitting the LyP-1 peptide.

PLL–PEG and PLL–PEG–LyP-1 Synthesis. OPSS–PEG–SVA was added to 1–5 kDa poly-L-lysine (Sigma-Aldrich) to modify 5% of lysines. The mixture was reacted for 1 h at room temperature in PBS. A total of 1.2 equiv of cysteine-bearing LyP-1 was added and reacted overnight. Unreacted LyP-1 was removed using a PD-10 desalting column. PLL–PEG was synthesized by omitting the LyP-1 peptide.

Nanoparticle Formulation. All siRNA, PEG-containing components, and peptides were resuspended as concentrated stocks in nuclease-free water (Life Technologies). Particles were formulated by mixing the siRNA, PEG-containing component, and peptide in 1:1:2 volumetric ratios, first by thoroughly mixing the siRNA with the PEG and by subsequently mixing in the peptide to create a concentrated solution of TPNs. Finally, this solution was adjusted to the desired dilution and buffer composition with appropriate diluent.

Dynamic Light Scattering and Electrophoretic Light Scattering. TPNs were formulated at 15:1 peptide–siRNA molar ratios and 0–15:1 PEG–siRNA. RNase-free PBS (10×,

pH 7.4; Life Technologies) was added after particle formation to achieve 1× PBS and a final siRNA concentration of 200 nM. Hydrodynamic diameters were obtained using a DynaPro Plate Reader (Wyatt Technology) to analyze 50 μL of each sample (n = 3 per condition). To measure ζ potentials, TPNs were formulated as above for a final siRNA concentration of 1 μM in 55 μL of 1× PBS (pH 7.4) and then diluted to 800 μL with nuclease-free water. The ζ potential was then measured via electrophoretic light scattering using a ZetaSizer Nano ZS90 instrument (Malvern).

Transmission Electron Microscopy. pTP–PEG and DSPE–PEG TPNs (15:15:1) were formed in PBS as described above, adhered to charged grids, and negatively stained with 2% uranyl acetate on the TEM grid. They were imaged on an FEI Tecnai Spirit TEM operated at 80 kV.

Gel Mobility Shift Assay. TPNs were formed at the specified ratios for a final concentration of 200 nM siRNA (DyLight 677-siLuc) in 1× PBS. A total of 10 μL of each TPN sample or free siRNA was mixed with 2 μL of 30% glycerol and loaded into a 2% agarose gel. The gel was run at 100 V for 45 min in 1× TAE buffer, and siRNA fluorescence was imaged on a LI-COR Odyssey infrared scanner. Signal was quantified using ImageJ.

Polyanion-Exchange Gel Electrophoresis. TPNs were formulated as above at a 15:15:1 peptide–PEG–siRNA ratio at a final DyLight 677-siLuc concentration of 200 nM, and polyglutamic acid (Sigma; 3000–15 000 molecular weight) was added postformulation for a final molar ratio of 0–480:1 polyglutamic acid–siRNA. The particles were incubated for 15 min at room temperature prior to gel mobility shift assay, performed as above.

Cell Culture. OVCAR-8 cells stably expressing firefly luciferase (OVCAR-8 Luc[+]) were a generous gift from the lab of Joyce Liu (Dana Farber Cancer Center). They were cultured in RPMI 1640 media with 10% FBS and 100 U/mL penicillin and streptomycin. Unless stated otherwise, OVCAR-8 Luc^{+} cells were plated in 96 well plates with 8000 cells per well 24 h prior to the start of each experiment. MDA-MB-435 cells (ATCC) were grown in DMEM with 10% FBS and 100 U/mL penicillin and streptomycin.

Transfection. For all in vitro transfection assays, TPNs were formed at the specified ratios for a final concentration of 100 nM siRNA in Opti-MEM serum-free media (Life Technologies, Gibco). TAMRA-labeled tandem peptide was used to allow tracking and quantification on microscopy and flow cytometry. Cells were dosed in 96 well plates by the removal of growth media and addition of 100 nM TPN solution (n = 4 per condition). After 4–6 h of incubation at 37 °C, media was replaced with RPMI 1640 supplemented with 10% fetal bovine serum for a further 20 h.

Luciferase Knockdown. OVCAR-8 Luc^{+} cells were transfected with 100 nM siLuc using the standard protocol above. A total of 48 h after transfection, luciferase activity was assessed using the firefly Luciferase Assay System (Promega), and the protein content of each well was determined using the bicinchoninic acid assay (Pierce). Bioluminescent signal was quantified on an Infinite M200 Pro plate reader (Tecan) and normalized by total protein content of each well.

Microscopy. OVCAR-8 cells were plated at 8000 cells per well on black glass-bottom 96 well plates precoated for 30 min with 100 μg/mL rat tail collagen (Becton Dickinson Biosciences). Cells were transfected with TPNs at the stated ratios with a final concentration of 100 nM DyLight 647-siRNA. After

24 h, cells were rinsed with CellScrub Buffer (Genlantis) to remove nonspecifically adsorbed materials and fixed with 4% paraformaldehyde. Cells were stained with Alexa Fluor 488 conjugated phalloidin (Invitrogen) according to manufacturer's instructions.

Uptake Flow Cytometry. OVCAR-8 cells were transfected in a 96 well plate as described above ($n = 4$ per condition). A total of 24 h after the start of transfection, cells were trypsinized and brought to single-cell suspension in 100 μL PBS + 2% FBS. TAMRA-peptide fluorescence (561/582) and VivoTag-S750-siLuc fluorescence (640/780) in live single cells was measured on a BD LSR II flow cytometer and analyzed using FlowJo software.

Circulation Time. Swiss Webster mice were intravenously (tail vein) injected under isoflurane anesthesia with non-PEGylated TPNs, 15:15:1 pTP−PEG TPNs, or 15:15:1 pTP−PEG−LyP-1 TPNs at 0.5 nmol siRNA dose per mouse ($n = 5$ per condition). VivoTag-S750 siRNA was used to minimize interference from autofluorescent background. Retro-orbital blood draws (10 μL each) were taken at 1, 10, 20, 40, 80, and 160 min time points following injection using heparinized glass capillaries (VWR) and scanned using a LI-COR Odyssey near-infrared scanner. Fluorescence was quantified using ImageJ and converted to blood concentrations using a standard curve of ex vivo blood samples spiked with known concentrations of VivoTag-labeled siRNA.

Complement Activation Assay. The three particle formulations above were incubated with human plasma (Pacific Hemostasis Normal Coagulation Control Plasma) at a final concentration of 0.25 μM siRNA for 30 min at 37 °C on a rocking platform. Subsequently, C3a/C3a-desArg and C5a/C5a-desArg concentrations in the plasma were determined via ELISA (MicroVue C3a Plus EIA and MicroVue C5a EIA, Quidel, respectively) according to manufacturer instructions.

Organ Biodistribution. NCR−nude mice were implanted with MDA-MB-435 xenografts subcutaneously (5×10^6 cells per flank, bilaterally), and tumors were allowed to grow for approximately 1 month until the primary axis diameter reached ~5 mm. The mice were then injected intravenously in the same manner and with the same dose as for the circulation time study using VivoTag-S750 labeled siRNA ($n = 7$ per condition). After 3 h, mice were euthanized, and necropsy was performed to remove the lungs, heart, left kidney, one liver lobe, spleen, and both tumors. Organs were scanned using a LI-COR Odyssey near-infrared scanner (LI-COR Biosciences), and analysis of average fluorescence intensity was performed in ImageJ.

Statistical Analysis. Knockdown data and ζ potentials were analyzed by one-way ANOVA with a Tukey post-test. siRNA uptake, circulation time, and organ biodistribution were analyzed by two-way ANOVA with a Bonferroni post-test. All statistical analyses were performed using GraphPad Prism software.

ASSOCIATED CONTENT

Ⓢ Supporting Information

The Supporting Information is available free of charge on the ACS Publications website at DOI: 10.1021/acs.bioconjchem.6b00304.

Figures showing expected chemical structures of the modular PEG components, siRNA cargo encapsulation efficiency in PEG TPNs, TEM micrographs, serum stability of PEG TPNs, polyanion exchange gel electrophoresis, and complement activation. (PDF)

AUTHOR INFORMATION

Corresponding Author

*E-mail: sbhatia@mit.edu.

Author Contributions

[#]J.H.L and E.J.K. contributed equally to this manuscript.

Notes

The authors declare no competing financial interest.

REFERENCES

(1) Pecot, C. V., Calin, G. A., Coleman, R. L., Lopez-Berestein, G., and Sood, A. K. (2011) RNA interference in the clinic: challenges and future directions. *Nat. Rev. Cancer 11*, 59−67.

(2) Ginn, S. L., Alexander, I. E., Edelstein, M. L., Abedi, M. R., and Wixon, J. (2013) Gene therapy clinical trials worldwide to 2012 - an update. *Journal of Gene Medicine 15*, 65−77.

(3) Doudna, J. A., and Charpentier, E. (2014) Genome editing. The new frontier of genome engineering with CRISPR-Cas9. *Science 346*, 1258096.

(4) Ren, Y., Cheung, H. W., von Maltzhan, G., Agrawal, A., Cowley, G. S., Weir, B. A., Boehm, J. S., Tamayo, P., Karst, A. M., Liu, J. F., et al. (2012) Targeted tumor-penetrating siRNA nanocomplexes for credentialing the ovarian cancer oncogene ID4. *Sci. Transl. Med. 4*, 147ra112.

(5) Teesalu, T., Sugahara, K. N., and Ruoslahti, E. (2013) Tumor-penetrating peptides. *Front. Oncol. 3*, 216.

(6) Pooga, M., Kut, C., Kihlmark, M., Hällbrink, M., Fernaeus, S., Raid, R., Land, T., Hallberg, E., Bartfai, T., and Langel, U. (2001) Cellular translocation of proteins by transportan. *FASEB J. 15*, 1451−1453.

(7) Lin, K. Y., Kwon, E. J., Lo, J. H., and Bhatia, S. N. (2014) Drug-induced amplification of nanoparticle targeting to tumors. *Nano Today 9*, 550−559.

(8) Park, J.-H., von Maltzahn, G., Xu, M. J., Fogal, V., Kotamraju, V. R., Ruoslahti, E., Bhatia, S. N., and Sailor, M. J. (2010) Cooperative nanomaterial system to sensitize, target, and treat tumors. *Proc. Natl. Acad. Sci. U. S. A. 107*, 981−986.

(9) Uchida, M., Kosuge, H., Terashima, M., Willits, D. A., Liepold, L. O., Young, M. J., McConnell, M. V., and Douglas, T. (2011) Protein Cage Nanoparticles Bearing the LyP-1 Peptide for Enhanced Imaging of Macrophage-Rich Vascular Lesions. *ACS Nano 5*, 2493−2502.

(10) Seo, J. W., Baek, H., Mahakian, L. M., Kusunose, J., Hamzah, J., Ruoslahti, E., and Ferrara, K. W. (2014) 64Cu-Labeled LyP-1-Dendrimer for PET-CT Imaging of Atherosclerotic Plaque. *Bioconjugate Chem. 25*, 231−239.

(11) Pack, D. W., Hoffman, A. S., Pun, S., and Stayton, P. S. (2005) Design and development of polymers for gene delivery. *Nat. Rev. Drug Discovery 4*, 581−593.

(12) Aied, A., Greiser, U., Pandit, A., and Wang, W. (2013) Polymer gene delivery: overcoming the obstacles. *Drug Discovery Today 18*, 1090−8.

(13) Ren, Y., Hauert, S., Lo, J. H., and Bhatia, S. N. (2012) Identification and characterization of receptor-specific peptides for siRNA delivery. *ACS Nano 6*, 8620−8631.

(14) Sato, A., Choi, S. W., Hirai, M., Yamayoshi, A., Moriyama, R., Yamano, T., Takagi, M., Kano, A., Shimamoto, A., and Maruyama, A. (2007) Polymer brush-stabilized polyplex for a siRNA carrier with long circulatory half-life. *J. Controlled Release 122*, 209−16.

(15) Knop, K., Hoogenboom, R., Fischer, D., and Schubert, U. S. (2010) Poly(ethylene glycol) in drug delivery: pros and cons as well as potential alternatives. *Angew. Chem., Int. Ed. 49*, 6288−308.

(16) Davis, M. E., Zuckerman, J. E., Choi, C. H. J., Seligson, D., Tolcher, A., Alabi, C. A., Yen, Y., Heidel, J. D., and Ribas, A. (2010) Evidence of RNAi in humans from systemically administered siRNA via targeted nanoparticles. *Nature 464*, 1067−1070.

(17) Love, K. T., Mahon, K. P., Levins, C. G., Whitehead, K. A., Querbes, W., Dorkin, J. R., Qin, J., Cantley, W., Qin, L. L., Racie, T., et al. (2010) Lipid-like materials for low-dose, in vivo gene silencing. *Proc. Natl. Acad. Sci. U. S. A. 107*, 1864−9.

(18) Akinc, A., Zumbuehl, A., Goldberg, M., Leshchiner, E. S., Busini, V., Hossain, N., Bacallado, S. A., Nguyen, D. N., Fuller, J., Alvarez, R., et al. (2008) A combinatorial library of lipid-like materials for delivery of RNAi therapeutics. *Nat. Biotechnol. 26*, 561−9.

(19) Malek, A., Merkel, O., Fink, L., Czubayko, F., Kissel, T., and Aigner, A. (2009) In vivo pharmacokinetics, tissue distribution and underlying mechanisms of various PEI(-PEG)/siRNA complexes. *Toxicol. Appl. Pharmacol. 236*, 97−108.

(20) Jhaveri, A. M., and Torchilin, V. P. (2014) Multifunctional polymeric micelles for delivery of drugs and siRNA, *Front. Pharmacol.,* 5,10.3389/fphar.2014.00077

(21) Morris, M. C., Gros, E., Aldrian-Herrada, G., Choob, M., Archdeacon, J., Heitz, F., and Divita, G. (2007) A non-covalent peptide-based carrier for in vivo delivery of DNA mimics. *Nucleic Acids Res. 35*, e49.

(22) Jokerst, J. V., Lobovkina, T., Zare, R. N., and Gambhir, S. S. (2011) Nanoparticle PEGylation for imaging and therapy. *Nanomedicine 6*, 715−28.

(23) Lin, K. Y., Lo, J. H., Consul, N., Kwong, G. A., and Bhatia, S. N. (2014) Self-titrating anticoagulant nanocomplexes that restore homeostatic regulation of the coagulation cascade. *ACS Nano 8*, 8776−85.

(24) von Maltzahn, G., Park, J. H., Agrawal, A., Bandaru, N. K., Das, S. K., Sailor, M. J., and Bhatia, S. N. (2009) Computationally guided photothermal tumor therapy using long-circulating gold nanorod antennas. *Cancer Res. 69*, 3892−900.

(25) Hashizume, H., Baluk, P., Morikawa, S., McLean, J. W., Thurston, G., Roberge, S., Jain, R. K., and McDonald, D. M. (2000) Openings between defective endothelial cells explain tumor vessel leakiness. *Am. J. Pathol. 156*, 1363−80.

(26) Jain, R. K., and Stylianopoulos, T. (2010) Delivering nano-medicine to solid tumors. *Nat. Rev. Clin. Oncol. 7*, 653−664.

(27) Mishra, S., Webster, P., and Davis, M. E. (2004) PEGylation significantly affects cellular uptake and intracellular trafficking of non-viral gene delivery particles. *Eur. J. Cell Biol. 83*, 97−111.

(28) Qhattal, H. S., Hye, T., Alali, A., and Liu, X. (2014) Hyaluronan polymer length, grafting density, and surface poly(ethylene glycol) coating influence in vivo circulation and tumor targeting of hyaluronan-grafted liposomes. *ACS Nano 8*, 5423−40.

(29) Nelson, C. E., Kintzing, J. R., Hanna, A., Shannon, J. M., Gupta, M. K., and Duvall, C. L. (2013) Balancing cationic and hydrophobic content of PEGylated siRNA polyplexes enhances endosome escape, stability, blood circulation time, and bioactivity in vivo. *ACS Nano 7*, 8870−80.

(30) Gao, S., Dagnaes-Hansen, F., Nielsen, E. J., Wengel, J., Besenbacher, F., Howard, K. A., and Kjems, J. (2009) The effect of chemical modification and nanoparticle formulation on stability and biodistribution of siRNA in mice. *Mol. Ther. 17*, 1225−33.

(31) Zuckerman, J. E., Choi, C. H. J., Han, H., and Davis, M. E. (2012) Polycation-siRNA nanoparticles can disassemble at the kidney glomerular basement membrane. *Proc. Natl. Acad. Sci. U. S. A. 109*, 3137−3142.

(32) Hamad, I., Al-Hanbali, O., Hunter, A. C., Rutt, K. J., Andresen, T. L., and Moghimi, S. M. (2010) Distinct polymer architecture mediates switching of complement activation pathways at the nanosphere-serum interface: implications for stealth nanoparticle engineering. *ACS Nano 4*, 6629−38.

(33) Verhoef, J. J., Carpenter, J. F., Anchordoquy, T. J., and Schellekens, H. (2014) Potential induction of anti-PEG antibodies and complement activation toward PEGylated therapeutics. *Drug Discovery Today 19*, 1945−52.

(34) Wibroe, P. P., and Moghimi, S. M. (2012) Complement Sensing of Nanoparticles and Nanomedicines. In *Functional Nanoparticles for Bioanalysis, Nanomedicine, and Bioelectronic Devices*, pp 365−382, vol 2, American Chemical Society, Washington, DC.

(35) Moghimi, S. M., Andersen, A. J., Ahmadvand, D., Wibroe, P. P., Andresen, T. L., and Hunter, A. C. (2011) Material properties in complement activation. *Adv. Drug Delivery Rev. 63*, 1000−1007.

(36) Choi, C. H., Alabi, C. A., Webster, P., and Davis, M. E. (2010) Mechanism of active targeting in solid tumors with transferrin-containing gold nanoparticles. *Proc. Natl. Acad. Sci. U. S. A. 107*, 1235−40.

(37) Srinivasarao, M., Galliford, C. V., and Low, P. S. (2015) Principles in the design of ligand-targeted cancer therapeutics and imaging agents. *Nat. Rev. Drug Discovery 14*, 203−19.

(38) Daniels, T. R., Delgado, T., Helguera, G., and Penichet, M. L. (2006) The transferrin receptor part II: targeted delivery of therapeutic agents into cancer cells. *Clin. Immunol. (Amsterdam, Neth.) 121*, 159−76.

(39) Akinc, A., Querbes, W., De, S., Qin, J., Frank-Kamenetsky, M., Jayaprakash, K. N., Jayaraman, M., Rajeev, K. G., Cantley, W. L., Dorkin, J. R., et al. (2010) Targeted Delivery of RNAi Therapeutics With Endogenous and Exogenous Ligand-Based Mechanisms. *Mol. Ther. 18*, 1357−64.

(40) Nie, S. (2010) Understanding and overcoming major barriers in cancer nanomedicine. *Nanomedicine 5*, 523−8.

Supporting Information

Comparison of Modular PEG Incorporation Strategies for Stabilization of Peptide-siRNA Nanocomplexes

Justin H. Lo,[†,‡,#] Ester J. Kwon,[†,#] Angela Q. Zhang,[†,‡] Preeti Singhal,[†] and Sangeeta N. Bhatia[*,†,‡,§,‖,⊥]

† Koch Institute for Integrative Cancer Research, MIT, 500 Main Street, Cambridge, Massachusetts 02139, United States
‡ Harvard−MIT Division of Health Sciences and Technology and § Department of Electrical Engineering and Computer Science, MIT, 77 Massachusetts Avenue, Cambridge, Massachusetts 02139, United States
‖ Department of Medicine, Brigham and Women's Hospital, 75 Francis Street, Boston, Massachusetts 02115, United States
⊥ Howard Hughes Medical Institute, 4000 Jones Bridge Road, Chevy Chase, Maryland 20815, United States

# These authors contributed equally to this manuscript
* Corresponding author
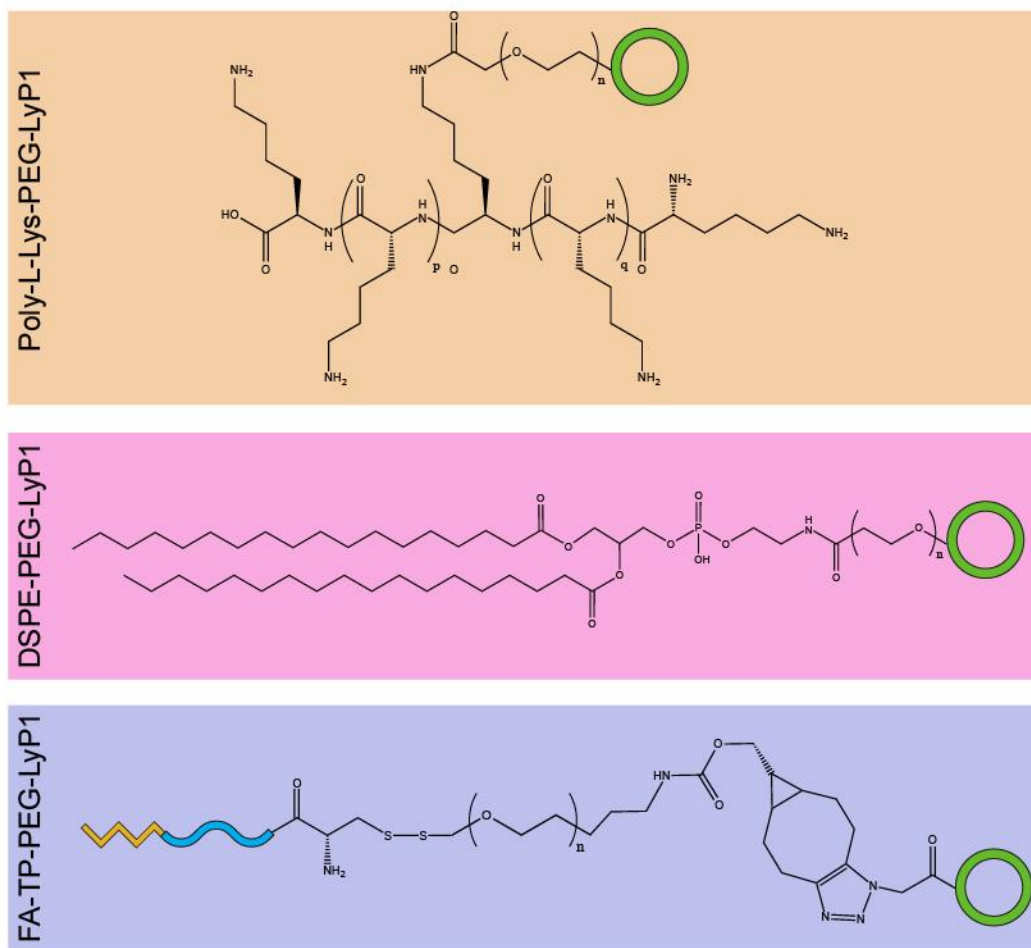
Figure S1. Expected chemical structures of the modular PEG components. The green circle indicates the position of the cyclic LyP-1 peptide, if added.
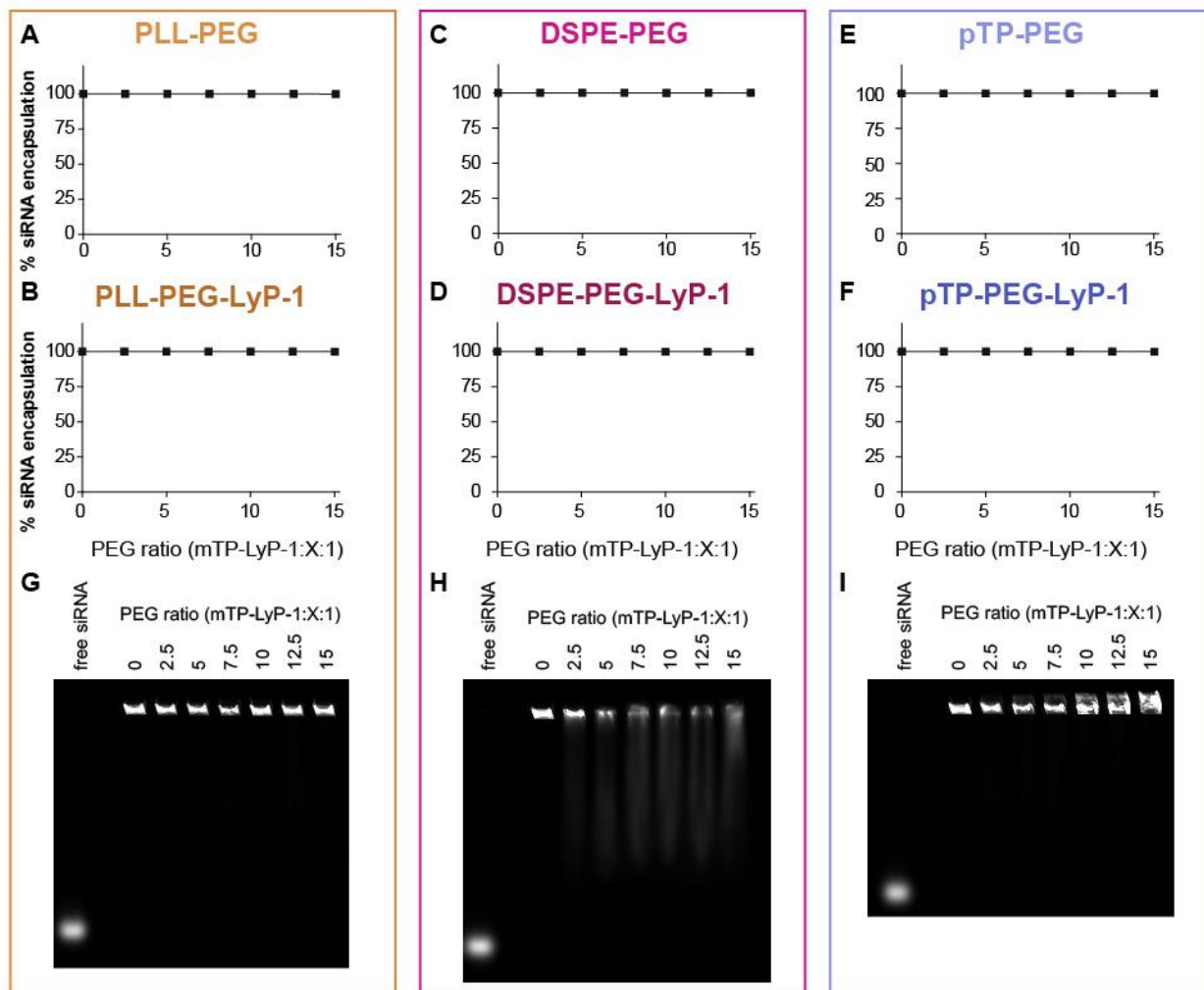
Figure S2. siRNA cargo encapsulation efficiency in PEG TPNs (A-F) Percentage of free siRNA encapsulated by PEG-containing TPNs, as quantified from an electrophoresis mobility shift assay in agarose gels. Scans of agarose gels used for analysis are shown for PLL-PEG-LyP-1 **(G)**, DSPE-PEG-LyP-1 **(H)**, and pTP-PEG-LyP-1 **(I)**. While very small nanocomplexes could migrate in the gel, with direction dependent on net charge, in no cases was there a free siRNA band that runs with the free siRNA control in the left lane of each gel.
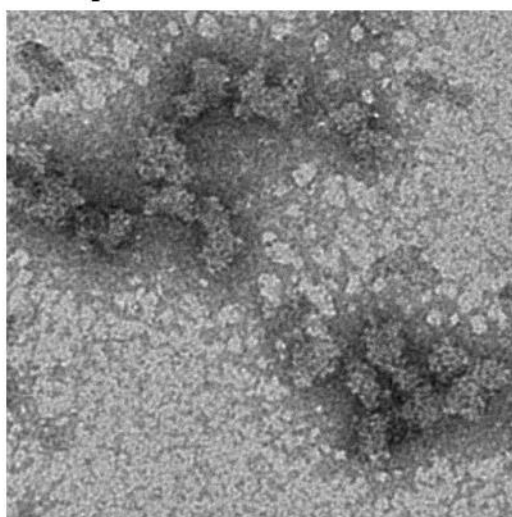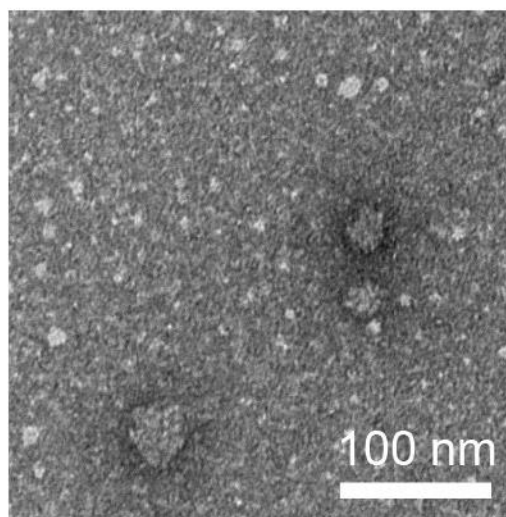
Figure S3. TEM micrographs. Negatively-stained TEMs of 15:15:1 pTP-PEG TPNs (left) and 15:15:1 DSPE-PEG TPNs (right) formed in 1x PBS.
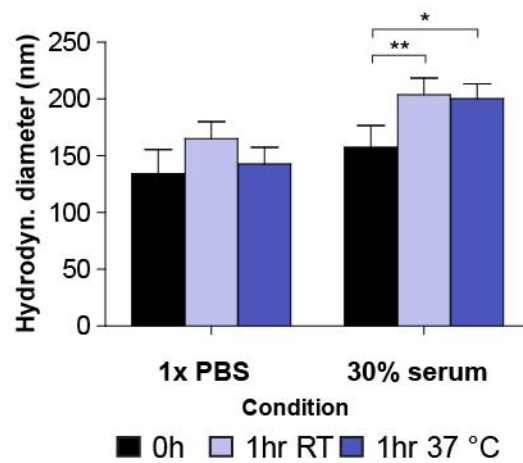
Figure S4. Serum stability of PEG TPNs. Diameters of 15:15:1 mTP-LyP-1:pTP-PEG-LyP-1:siRNA particles in isotonic buffer or 30% exosome-free FBS at room temperature or physiologic temperature. Statistical significance evaluated by two-way ANOVA with Bonferroni post-test. *: p<0.05, **: p<0.01.
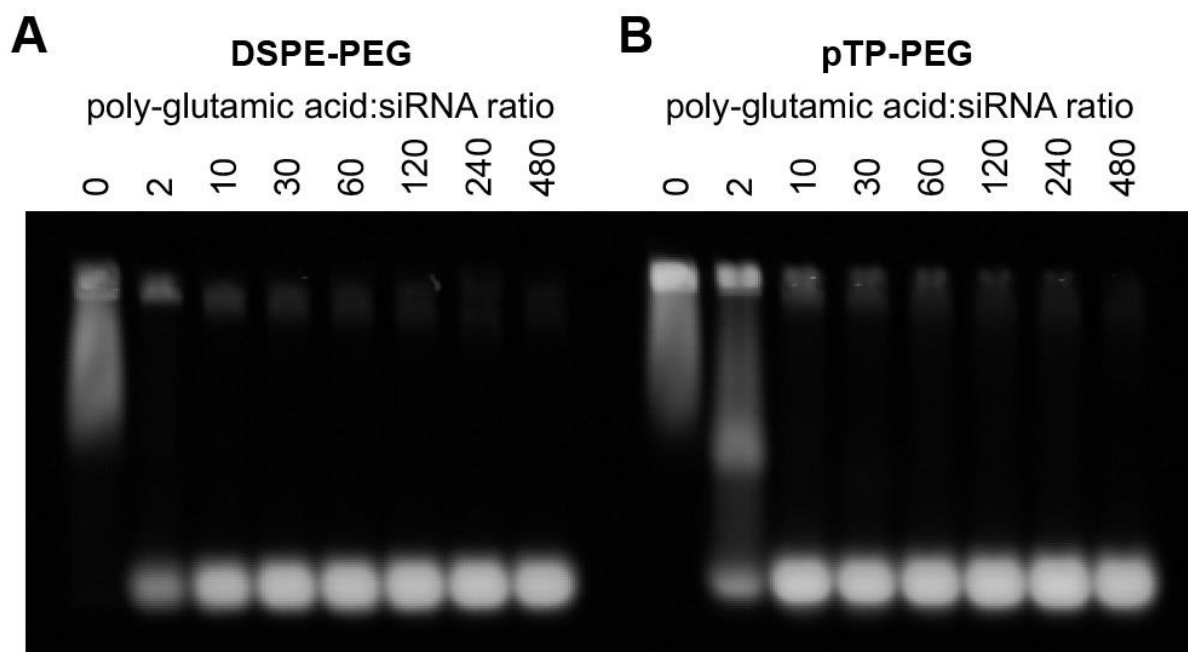
Figure S5. Polyanion exchange gel electrophoresis. PEG TPNs formed with **(A)** DSPE-PEG or **(B)** pTP-PEG were mixed with increasing molar ratios of poly-glutamic acid to siRNA (with the concentration of the particles held constant). Appearance of the free siRNA band (bottom) and loss of siRNA retained in the loading wells (top) corresponds with the degree of particle disruption and displacement of siRNA by poly-glutamic acid.
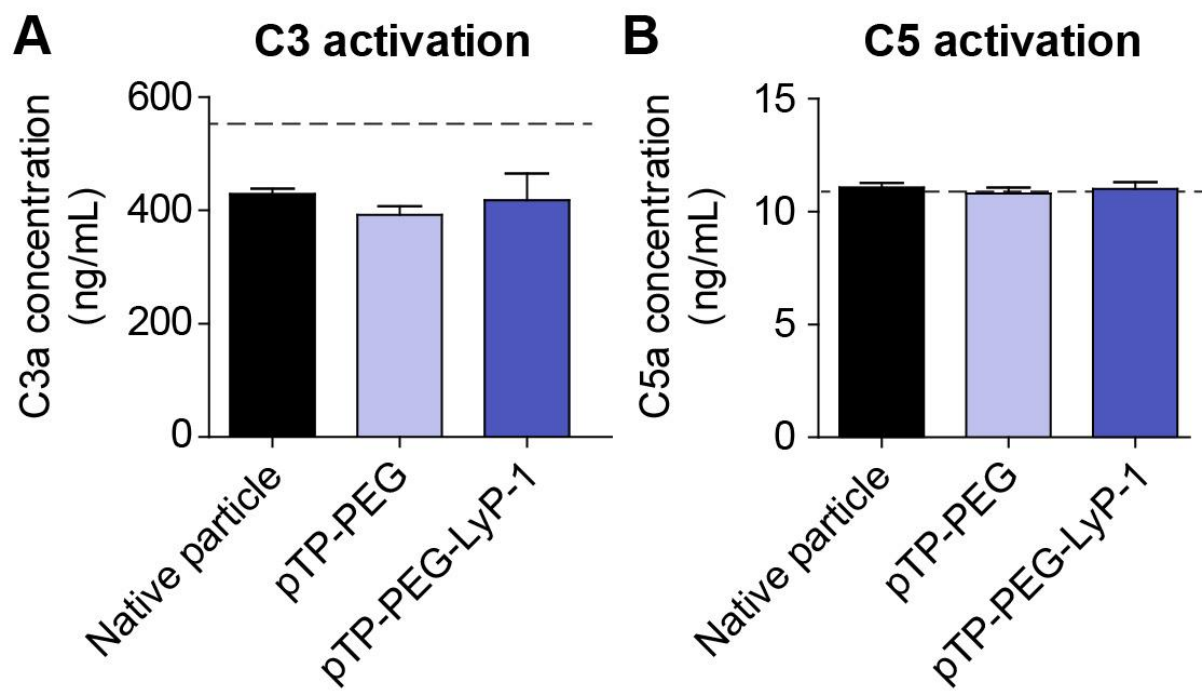
Figure S6. Complement activation. Levels of **(A)** C3a or C3a-desArg and **(B)** C5a or C5a-desArg after incubation of non-PEGylated TPNs (15:1 peptide:siRNA ratio), pTP-PEG TPNs (15:15:1), or pTP-PEG-LyP-1 particles (15:15:1) with human plasma.